

Nonadiabatic holonomic quantum computation in decoherence-free subspaces on Rydberg atoms

Ya Gao(郜雅), Meng-Le Guo(郭梦乐), Pei-Yao Song(宋佩瑶), Ji-Ze Han(韩济泽), Zhi-Guo Huang(黄智国), Jin-Lei Wu(吴金雷), and Shi-Lei Su(苏石磊)

Citation: Chin. Phys. B, 2026, 35 (**8**): 080301. DOI: 10.1088/1674-1056/ae6cce
http://cpb.iphy.ac.cn; http://iopscience.iop.org/cpb

What follows is a list of articles you may be interested in

Enhancing the performance of quantum battery by squeezing reservoir engineering

Yue Li(李月), Rong-Fang Liu(刘蓉芳), Jia-Bin You(游佳斌), Wan-Li Yang(杨万里), and Hua Guan(管桦)
Chin. Phys. B, 2026, 35 (**1**): 010303. DOI: 10.1088/1674-1056/ae1df2

Adiabatic holonomic quantum computation in decoherence-free subspaces with two-body interaction

Xiaoyu Sun(孙晓雨), Lei Qiao(乔雷), and Peizi Zhao(赵培茊)
Chin. Phys. B, 2025, 34 (**9**): 090308. DOI: 10.1088/1674-1056/adeb5e

Bayesian phase difference estimation based on single-photon projective measurement

Xu-Hao Yu(余旭豪), Ying Wei(韦颖), Ran Yang(杨然), Wen-Hui Song(宋文慧), Yingning Miao(缪应宁), Wei Zhou(周唯), Xinhui Li(李新慧), Xiaoqin Gao(高小钦), Yan-Xiao Gong(龚彦晓), and Shi-Ning Zhu(祝世宁)
Chin. Phys. B, 2025, 34 (**7**): 070305. DOI: 10.1088/1674-1056/adde33

Correcting on-chip distortion of control pulses with silicon spin qubits

Ming Ni(倪铭), Rong-Long Ma(马荣龙), Zhen-Zhen Kong(孔真真), Ning Chu(楚凝), Wei-Zhu Liao(廖伟筑), Sheng-Kai Zhu(祝圣凯), Chu Wang(王储), Gang Luo(罗刚), Di Liu(刘頔), Gang Cao(曹刚), Gui-Lei Wang(王桂磊), Hai-Ou Li(李海欧), and Guo-Ping Guo(郭国平)
Chin. Phys. B, 2025, 34 (**1**): 010308. DOI: 10.1088/1674-1056/ad8db1

Established conversions for hybrid entangled states assisted by error-predicted parity-discriminated devices

Fang-Fang Du(杜芳芳), Zhi-Guo Fan(范志国), Xue-Mei Ren(任雪梅), Ming Ma(马明), and Wen-Yao Liu(刘文耀)
Chin. Phys. B, 2025, 34 (**1**): 010303. DOI: 10.1088/1674-1056/ad8fa0

SPECIAL TOPIC — Quantum frontiers with Rydberg atoms

Nonadiabatic holonomic quantum computation in decoherence-free subspaces on Rydberg atoms

Ya Gao(郜雅)[1], Meng-Le Guo(郭梦乐)[1], Pei-Yao Song(宋佩瑶)[1], Ji-Ze Han(韩济泽)[4], Zhi-Guo Huang(黄智国)[4], Jin-Lei Wu(吴金雷)[1,2,†], and Shi-Lei Su(苏石磊)[1,3,‡]

[1] *School of Physics, Zhengzhou University, Zhengzhou* 450001, *China*
[2] *Institute of Quantum Science and Technology, Yanbian University, Yanji* 133002, *China*
[3] *Institute of Quantum Materials and Physics, Henan Academy of Science, Zhengzhou* 450046, *China*
[4] *China Mobile (Suzhou) Software Technology Co., Ltd., Suzhou* 215163, *China*

(Received 9 March 2026; revised manuscript received 29 April 2026; accepted manuscript online 13 May 2026)

We propose a scheme for realizing nonadiabatic holonomic quantum computation within a decoherence-free subspace using Rydberg atoms. By employing large-detuned lasers and the Rydberg antiblockade condition, we construct an effective Hamiltonian that couples logical states in a three-atom decoherence-free subspace while ensuring that the Rydberg states remain unpopulated. This approach significantly suppresses decoherence caused by atomic spontaneous emission and mitigates the mechanical effects and sensitivity to interatomic distance variations associated with Rydberg excitations. We demonstrate the realization of both conventional and single-loop single-logical-qubit holonomic gates with high fidelity. Furthermore, by utilizing an asymmetric encoding method, in which the control logical qubits employ Rydberg-state encoding to provide the required conditional blockade, we extend the scheme to construct universal two- and three-logical-qubit holonomic gates, offering a robust and scalable approach for quantum information processing.

Keywords: quantum computation, Rydberg atom, geometric phase, decoherence-free subspace

PACS: 03.67.Lx, 03.67.–a, 32.80.Ee, 03.67.Pp

DOI: 10.1088/1674-1056/ae6cce **CSTR:** 32038.14.CPB.ae6cce

1. Introduction

Rydberg atoms, when excited to Rydberg states, exhibit large dipole moments and generate Rydberg–Rydberg interactions (RRIs).[1–7] RRIs have been directly measured in experiments and have led to the observation of the Rydberg blockade phenomenon.[2,3,8,9] Based on RRIs, several quantum information processing tasks have been studied, including the preparation of quantum entangled states,[10–13] the construction of quantum logic gates,[14–17] quantum simulators,[18–20] quantum algorithms,[21–23] quantum metrology,[24–26] and quantum repeaters.[27–29]

Early in 1984, Berry found that a quantum system with a nondegenerate eigenstate acquires a geometric phase when it undergoes adiabatic cyclic evolution.[30] Shortly thereafter, the geometric phase of quantum systems with degenerate eigenstates undergoing adiabatic cyclic evolution was investigated,[31] and nonadiabatic evolutions of quantum systems with nondegenerate[32] and degenerate[33] eigenvectors were studied, respectively. Subsequently, the first geometric quantum computation scheme based on the Abelian geometric phase and adiabatic processes was presented.[34] The adiabatic holonomic quantum computation was then proposed based on adiabatic evolution and non-Abelian geometric phases.[35,36] Quantum computation based on nonadiabatic Abelian geometric phases was also studied.[37,38] In addition, nonadiabatic holonomic quantum computation (NHQC) based on nonadiabatic non-Abelian geometric phases was proposed.[39,40] On the one hand, NHQC possesses a geometric nature that provides tolerance against certain control errors. On the other hand, NHQC does not need to satisfy the adiabatic condition, which can reduce the influence of dissipation by avoiding the requirement of long operation times. Experimentally, NHQC has been demonstrated in superconducting circuits,[41–43] nitrogen-vacancy centres,[44–46] NMR systems,[47] and trapped ions,[48] and has been extensively studied theoretically in Rydberg atom systems.[22,49–65]

Despite the remarkable progress in Rydberg-atom-based quantum information processing, practical quantum computation remains susceptible to decoherence induced by unwanted coupling between the system and its environment. The decoherence-free subspace (DFS)[66,67] provides an elegant approach to addressing this issue, as it exploits a set of physical states that are inherently immune to specific types of noise, such as collective dephasing. The combination of NHQC and DFS[40,68] has been extensively explored in various physical platforms, including superconducting circuits[69]

†Corresponding author. E-mail: jlwu517@zzu.edu.cn
‡Corresponding author. E-mail: slsu@zzu.edu.cn

© 2026 Chinese Physical Society and IOP Publishing Ltd. All rights, including for text and data mining, AI training, and similar technologies, are reserved.

and trapped-ion systems.[70] However, compared with the two platforms mentioned above, the Rydberg-atom platform features longer coherence times and stronger long-range interactions, enabling faster gates and flexible scalability without relying on fixed circuit couplings or collective motional modes. Therefore, realizing NHQC within a DFS using Rydberg atoms, which combines the advantages of all three paradigms, remains an important and timely goal.

In this work, we propose a scheme to implement NHQC within a DFS using Rydberg atoms. Specifically, we encode a logical qubit in a three-atom DFS spanned by $\{|001\rangle, |010\rangle, |100\rangle\}$, which is inherently immune to collective dephasing noise. By employing large-detuned laser fields and operating under the Rydberg antiblockade condition, we adiabatically eliminate all Rydberg states and derive an effective Hamiltonian that couples the logical states $|0\rangle_L$ and $|1\rangle_L$ through an auxiliary state $|a\rangle_L \equiv |010\rangle$. This effective dynamics enables the realization of both conventional and single-loop single-logical-qubit holonomic gates. To extend the scheme beyond single-qubit operations, we adopt an asymmetric encoding strategy for the control and target logical qubits and demonstrate how to construct universal two- and three-logical-qubit holonomic gates by exploiting conditional Rydberg blockade effects. Throughout the entire protocol, Rydberg states remain virtually unpopulated, which significantly suppresses errors caused by atomic spontaneous emission and reduces sensitivity to variations in interatomic distances. The combination of DFS encoding and Rydberg-state elimination thus provides a route toward quantum information processing with intrinsic robustness against decoherence in neutral-atom systems.

2. Basic framework

2.1. Decoherence-free subspace encoding

The simplest DFS immune to collective-dephasing noise is

$$S^D = \mathrm{Span}\{|001\rangle,\ |010\rangle,\ |100\rangle\}. \tag{1}$$

We encode the logical qubit as $|0\rangle_L \equiv |001\rangle$ and $|1\rangle_L \equiv |100\rangle$. Meanwhile, $|a\rangle_L \equiv |010\rangle$ is encoded as an auxiliary logical state. We consider a simple model to demonstrate that this encoding is immune to collective-dephasing noise. Suppose the dephasing-noise-induced Hamiltonian for each single atom is[67]

$$\hat{H}_{\mathrm{dni}} = \varepsilon_0(t)|0\rangle\langle 0| + \varepsilon_1(t)|1\rangle\langle 1|, \tag{2}$$

where $\varepsilon_0(t)$ and $\varepsilon_1(t)$ denote the energy shifts of the states $|0\rangle$ and $|1\rangle$, respectively, induced by external noise sources such as magnetic-field fluctuations and laser-induced AC Stark shifts. We rewrite it in the three-atom basis and restrict it to the logical-qubit subspace as

$$\hat{H}'_{\mathrm{dni}}(t) = [2\varepsilon_0(t) + \varepsilon_1(t)](|0\rangle_L\langle 0| + |1\rangle_L\langle 1| + |a\rangle_L\langle a|). \tag{3}$$

In the interaction picture, considering the commutation relation, the evolution operator of a system initially in the DFS can be expressed as

$$\hat{U} = \mathrm{e}^{-\mathrm{i}\int \hat{H}'_{\mathrm{dni}}(t)\,\mathrm{d}t}\,\mathrm{e}^{-\mathrm{i}\int \hat{H}_{\mathrm{sys}}(t)\,\mathrm{d}t}, \tag{4}$$

where $\hat{H}_{\mathrm{sys}}$ is the system Hamiltonian. Thus, the collective noise term $\mathrm{e}^{-\mathrm{i}\int \hat{H}'_{\mathrm{dni}}(t)\,\mathrm{d}t}$ only generates a global phase, which has no effect on the logical qubit encoded in the DFS.

2.2. System and effective Hamiltonian

The configuration of the single logical qubit is shown in Fig. 1(a), where three Rydberg atoms are required. Each Rydberg atom has one Rydberg state $|R\rangle$ and two ground states $|0\rangle$ and $|1\rangle$, as shown in Fig. 1(b). The coupling from $|0\rangle$ ($|1\rangle$) to the Rydberg state $|R\rangle$ of atom k ($k = 1,2,3$) is realized by lasers with Rabi frequencies Ω_{2k-1} (Ω_{2k}) and detunings Δ_{2k-1} (Δ_{2k}), respectively. In the interaction picture, the Hamiltonian of the system atoms is (setting $\hbar = 1$)

$$\begin{aligned}\hat{H}_{\mathrm{full}} =& \sum_{k=1}^{3}\left(\frac{\Omega_{2k-1}\,\mathrm{e}^{\mathrm{i}\Delta_{2k-1}t}}{2}|0\rangle_k\langle R| + \frac{\Omega_{2k}\,\mathrm{e}^{\mathrm{i}\Delta_{2k}t}}{2}|1\rangle_k\langle R| + \mathrm{H.c.}\right)\\ &+ \sum_{k=2}^{3} V_{k-1}|R\rangle_1\langle R|\otimes|R\rangle_k\langle R|.\end{aligned} \tag{5}$$

In the following, we assume $V_k = V$ for simplicity. If the following conditions are satisfied:

$$\begin{aligned}&\Delta_1 + \Delta_4 = V - \delta, \quad \Delta_2 + \Delta_3 = V - \delta,\\ &\Delta_2 = \Delta_4 = \Delta_6, \quad \Delta_1 = \Delta_3 = \Delta_5,\\ &|\Delta_2 - \Delta_1| \gg \Omega_k, \quad \{\Delta_1,\ \Delta_2\} \gg \delta \gg \Omega_1\Omega_2/\bar{\Delta},\end{aligned} \tag{6}$$

with $1/\bar{\Delta} = 1/2(1/\Delta_1 + 1/\Delta_2)$, the effective dynamics indicate that the system Hilbert space is divided into four independent subspaces under perturbation theory: $S^1 = \{|000\rangle\}$, $S^D = \{|001\rangle,\ |010\rangle,\ |100\rangle\}$, $S^{D1} = \{|011\rangle,\ |101\rangle,\ |110\rangle\}$, and $S^2 = \{|111\rangle\}$. After a frame rotation with respect to $\hat{U}_{\mathrm{R}}^{\dagger} = \mathrm{e}^{\mathrm{i}\sum_{k=2}^{3} V|R\rangle_1\langle R|\otimes|R\rangle_k\langle R|t}$, one possible effective Hamiltonian of the system can be obtained through perturbation theory as

$$\begin{aligned}\hat{H}_{\mathrm{eff}} =& \ \Omega_{0L}|001\rangle\langle 010| + \Omega_{1L}|100\rangle\langle 010| + \mathrm{H.c.}\\ &+ \hat{S}_{001} + \hat{S}_{010} + \hat{S}_{100},\end{aligned} \tag{7}$$

when the initial state is in the subspace S^D, where

$$\begin{aligned}\Omega_{0L} =& \frac{\Omega_1\Omega_2^*\Omega_3^*\Omega_4}{16\delta}\left(\frac{1}{\Delta_1} + \frac{1}{\Delta_4}\right)\left(\frac{1}{\Delta_2} + \frac{1}{\Delta_3}\right),\\ \Omega_{1L} =& \frac{\Omega_1\Omega_2^*\Omega_5^*\Omega_6}{16\delta}\left(\frac{1}{\Delta_1} + \frac{1}{\Delta_6}\right)\left(\frac{1}{\Delta_2} + \frac{1}{\Delta_5}\right),\end{aligned} \tag{8}$$

and

$$\begin{aligned}\hat{S}_{001} &= \Big[\frac{|\Omega_1|^2}{\Delta_1}+\frac{|\Omega_4|^2}{\Delta_4}+\frac{|\Omega_5|^2}{\Delta_5}+\frac{|\Omega_1|^2|\Omega_4|^2}{16\delta}\Big(\frac{1}{\Delta_1}+\frac{1}{\Delta_4}\Big)^2 \\ &\quad -\mathcal{E}_{1,4,5}\Big]|001\rangle\langle 001|, \\ \hat{S}_{010} &= \Big[\frac{|\Omega_2|^2}{\Delta_2}+\frac{|\Omega_3|^2}{\Delta_3}+\frac{|\Omega_5|^2}{\Delta_5}+\frac{|\Omega_2|^2|\Omega_5|^2}{16\delta}\Big(\frac{1}{\Delta_2}+\frac{1}{\Delta_5}\Big)^2 \\ &\quad +\frac{|\Omega_2|^2|\Omega_3|^2}{16\delta}\Big(\frac{1}{\Delta_2}+\frac{1}{\Delta_3}\Big)^2-\mathcal{E}_{2,3,5}\Big]|010\rangle\langle 010|, \\ \hat{S}_{100} &= \Big[\frac{|\Omega_1|^2}{\Delta_1}+\frac{|\Omega_3|^2}{\Delta_3}+\frac{|\Omega_6|^2}{\Delta_6}+\frac{|\Omega_1|^2|\Omega_6|^2}{16\delta}\Big(\frac{1}{\Delta_1}+\frac{1}{\Delta_6}\Big)^2 \\ &\quad -\mathcal{E}_{1,3,6}\Big]|100\rangle\langle 100|. \end{aligned} \tag{9}$$

We define

$$\mathcal{E}_{x,y,z} = \frac{1}{16}\Big(\frac{|\Omega_x|^2}{\Delta_x^2}+\frac{|\Omega_y|^2}{\Delta_y^2}+\frac{|\Omega_z|^2}{\Delta_z^2}\Big)\Big(\frac{|\Omega_x|^2}{\Delta_x}+\frac{|\Omega_y|^2}{\Delta_y}+\frac{|\Omega_z|^2}{\Delta_z}\Big).$$

For the three-atom basis $|abc\rangle$ in Eqs. (7) and (9), a, b, and c denote the states of atoms 3, 1, and 2, respectively. For this model, we introduce a detuning δ based on the conventional Rydberg antiblockade condition[71,72] and use high-order perturbation theory to adiabatically eliminate the two-excitation Rydberg states. Unlike conventional Rydberg blockade or antiblockade schemes, the collective states involving Rydberg excitations are eliminated in this approach. Consequently, the mechanical effects, sensitivity to variations in interatomic distances, and influence of atomic decay are significantly suppressed.

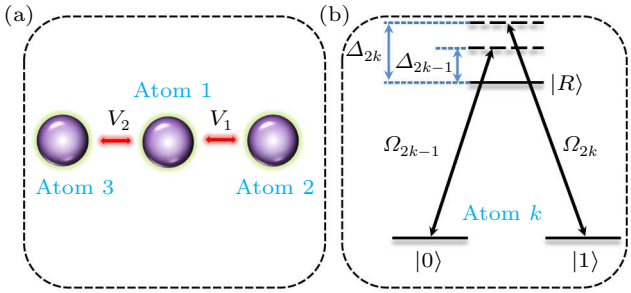


Fig. 1. (a) Configuration of three system atoms used to construct a single-logical-qubit encoding in the DFS. V_1 and V_2 denote the Rydberg–Rydberg interaction strengths. We assume that the neighboring RRIs are identical for simplicity. We then show that the non-neighboring RRI has a negligible effect on the scheme. (b) Each atom is driven by two blue-detuned lasers.

We then introduce additional large-detuned interactions on the state $|1\rangle$ of two atoms among the three atoms to generate Stark shifts for the states $|0\rangle_L$, $|1\rangle_L$, and $|a\rangle_L$. Without loss of generality, we consider an auxiliary energy level $|f\rangle_l$ coupled to $|1\rangle_l$ of atom l ($l=2,3$) with Rabi frequency Ω_{fl} and detuning Δ_{fl}. If the conditions

$$\Omega_{f2}^2/(4\Delta_{f2}) = C(\hat{S}_{010})-C(\hat{S}_{001}),$$

$$\Omega_{f3}^2/(4\Delta_{f3}) = C(\hat{S}_{010})-C(\hat{S}_{100}), \tag{10}$$

are satisfied, with $C(\hat{\mathcal{O}})$ denoting the coefficient of the operator $\hat{\mathcal{O}}$, the system Hamiltonian can be further simplified to

$$\hat{H}_{\rm eff} = \Omega_{0L}|0\rangle_L\langle a| + \Omega_{1L}|1\rangle_L\langle a| + \text{H.c.}, \tag{11}$$

by taking the completeness relation into account. In the following, we show how to realize NHQC in the Rydberg-atom DFS based on the constructed Hamiltonian in Eq. (11).

3. Single-qubit NHQC gate in Rydberg DFS

3.1. Conventional NHQC in Rydberg DFS

We consider all classical lasers to be square pulses, where Ω_1, Ω_2, Ω_3, and Ω_5 are real, while $\Omega_4 = \Omega_4' e^{i\varphi_4}$ and $\Omega_6 = \Omega_6' e^{i\varphi_6}$, with Ω_4', Ω_6', φ_4, and φ_6 being real. In this subsection, we set $\varphi_6 = 0$ and $\varphi_4 = \varphi$, and rewrite Hamiltonian (11) as

$$\hat{H}_{\rm eff} = \lambda\Big(\sin\frac{\theta}{2}e^{-i\varphi}|a\rangle_L\langle 0| + \cos\frac{\theta}{2}|a\rangle_L\langle 1|\Big) + \text{H.c.}, \tag{12}$$

where

$$\lambda = \sqrt{|\Omega_{0L}|^2+(\Omega_{1L})^2}, \quad \tan\frac{\theta}{2} = \frac{|\Omega_{0L}|}{\Omega_{1L}}. \tag{13}$$

The realization of NHQC can be clearly seen in the dressed-state representation, where the two lowest-energy states of Hamiltonian (12) are

$$\begin{aligned}|d\rangle_L &= \cos\frac{\theta}{2}|0\rangle_L - \sin\frac{\theta}{2}e^{-i\varphi}|1\rangle_L, \\ |b\rangle_L &= \sin\frac{\theta}{2}e^{i\varphi}|0\rangle_L + \cos\frac{\theta}{2}|1\rangle_L. \end{aligned} \tag{14}$$

The state $|d\rangle_L$ is the dark state and is decoupled from Hamiltonian (12). Therefore, Hamiltonian (12) can be viewed as $\lambda|a\rangle_L\langle b| + \text{H.c.}$, indicating that $|a\rangle_L$ only couples to the state $|b\rangle_L$ with the effective Rabi frequency λ.

Under the control of Eq. (12), $|b\rangle_L$ and $|d\rangle_L$ evolve as

$$\begin{aligned}|\psi_1(t)\rangle_L &= \hat{U}_1(t)|d\rangle_L = |d\rangle_L, \\ |\psi_2(t)\rangle_L &= \hat{U}_1(t)|b\rangle_L = \cos(\lambda t)|b\rangle_L - i\sin(\lambda t)|a\rangle_L. \end{aligned} \tag{15}$$

In the basis $\{|d\rangle_L, |b\rangle_L, |a\rangle_L\}$, this evolution operator has the matrix form

$$\hat{U}_1(t) = \begin{pmatrix} 1 & 0 & 0 \\ 0 & \cos(\lambda t) & -i\sin(\lambda t) \\ 0 & -i\sin(\lambda t) & \cos(\lambda t) \end{pmatrix}.$$

To realize NHQC, the cyclic condition and the parallel transport condition should be satisfied.[39,40] When $\lambda t = \pi$ is satisfied, the dressed states undergo cyclic evolution, since $|d\rangle_L$ remains invariant while $|b\rangle_L$ evolves to $-|b\rangle_L$, satisfying the cyclic condition. Moreover, one has $\langle\psi_i(t)|\hat{H}_{\rm eff}|\psi_j(t)\rangle = 0$ $(i,j=1,2)$. This result shows that the parallel transport

condition holds for arbitrary states in the evolving logical subspace. Based on this condition, the NHQC gate in the logical qubit subspace $\{|0\rangle_L, |1\rangle_L\}$ is constructed as

$$\hat{U}(\theta,\ \varphi) = \begin{pmatrix} \cos\theta & -\mathrm{e}^{\mathrm{i}\varphi}\sin\theta \\ -\mathrm{e}^{-\mathrm{i}\varphi}\sin\theta & -\cos\theta \end{pmatrix}, \tag{16}$$

where θ and φ are determined by the parameters of the laser pulses.

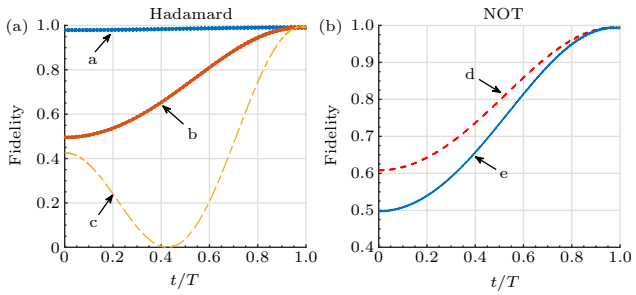


Fig. 2. Fidelity of the conventional single-qubit NHQC during one evolution period $T = \pi/\lambda$: (a) Hadamard gate and (b) NOT gate. The parameters are chosen as $V \simeq 57.407\Omega_1$, $\Delta_1 \simeq 16.667\Omega_1$, $\Delta_2 \simeq 38.889\Omega_1$, $\delta \simeq -1.852\Omega_1$, $\Omega_2 = \Omega_1$, $\Omega_3 = \Omega_4 = \sqrt{\sin(\theta/2)}\Omega_1$, and $\Omega_5 = \Omega_6 = \sqrt{\cos(\theta/2)}\Omega_1$. For the Hadamard gate with $\theta = \pi/4$ in (a), line a is obtained with $\vartheta = \pi/7$ and $\varphi = \pi$, line b with $\vartheta = \pi/4$ and $\varphi = \pi$, and line c with $\vartheta = \pi/4$ and $\varphi = \pi/8$. For the NOT gate with $\theta = \pi/2$ in (b), line d is obtained with $\vartheta = \pi/7$, while line e with $\vartheta = \pi/8$. The remaining parameters are chosen based on Eqs. (6) and (10).

If the initial state is set as $|\phi\rangle = \sin\vartheta|0\rangle_L + \cos\vartheta|1\rangle_L$, the ideal final state is given by $|\phi\rangle_{\mathrm{ide}} = \hat{U}(\theta,\ \varphi)|\phi\rangle$. On the other hand, the actual state $|\phi_{\mathrm{p}}\rangle$ can be obtained by numerically solving the Schrödinger equation. We use the definition $F = |\langle\phi_{\mathrm{p}}|\phi_{\mathrm{ide}}\rangle|^2$ to calculate the fidelity, as shown in Fig. 2.

3.2. Single-loop NHQC in Rydberg DFS

Although the holonomic gate in Eq. (16) is universal, it requires two applications, such as $\hat{U}(\pi/2,\ \Phi/2)\hat{U}(\pi/2,\ 0)$, to implement a phase gate with an arbitrary phase Φ. Thus, it is more interesting to generalize $\hat{U}$ to a more general case, i.e., realizing arbitrary unitary operations through single-loop evolution.[73] To this end, we divide the total evolution duration T into two equal intervals and set φ_4 and φ_6 as

$$\begin{cases} \varphi_4 = -\varphi, & \varphi_6 = \pi;\ t \in [0,\ T/2], \\ \varphi_4 = -\varphi + \gamma + \pi, & \varphi_6 = \gamma;\ t \in [T/2,\ T]. \end{cases} \tag{17}$$

One can easily verify that the cyclic and parallel transport conditions are also satisfied under this choice of parameters. The evolution operator in the basis $\{|0\rangle_L,\ |1\rangle_L\}$ is calculated as

$$\begin{aligned} &\hat{U}(\theta,\varphi,\gamma) \\ &= \mathrm{e}^{-\mathrm{i}\frac{\gamma}{2}} \begin{pmatrix} \cos\frac{\gamma}{2} - \mathrm{i}\cos\theta\sin\frac{\gamma}{2} & -\mathrm{i}\sin\frac{\gamma}{2}\sin\theta\,\mathrm{e}^{-\mathrm{i}\varphi} \\ -\mathrm{i}\sin\frac{\gamma}{2}\sin\theta\,\mathrm{e}^{\mathrm{i}\varphi} & \cos\frac{\gamma}{2} + \mathrm{i}\cos\theta\sin\frac{\gamma}{2} \end{pmatrix} \\ &= \mathrm{e}^{-\mathrm{i}\frac{\gamma}{2}} \cdot \mathrm{e}^{-\mathrm{i}\frac{\gamma}{2}\boldsymbol{n}\cdot\boldsymbol{\sigma}}, \end{aligned} \tag{18}$$

which corresponds to a rotation around the axis $\boldsymbol{n} = (\sin\theta\cos\varphi,\ \sin\theta\sin\varphi,\ \cos\theta)$ by an angle $\gamma/2$ and generates a set of universal single-qubit gates in the DFS after ignoring the global phase factor $\mathrm{e}^{-\mathrm{i}\gamma/2}$. The single-loop scheme enables arbitrary unitary operations by flexibly engineering the evolution path in parameter space, such that the accumulated geometric phase corresponds to an arbitrary SU(2) rotation. The performance of the single-loop universal gate is shown in Fig. 3. Three types of holonomic gates can achieve high fidelity at the end of evolution for specific initial states. To verify their effectiveness for arbitrary initial states, we simulate the average fidelity using the NOT gate as an example, as shown in Fig. 3(b).

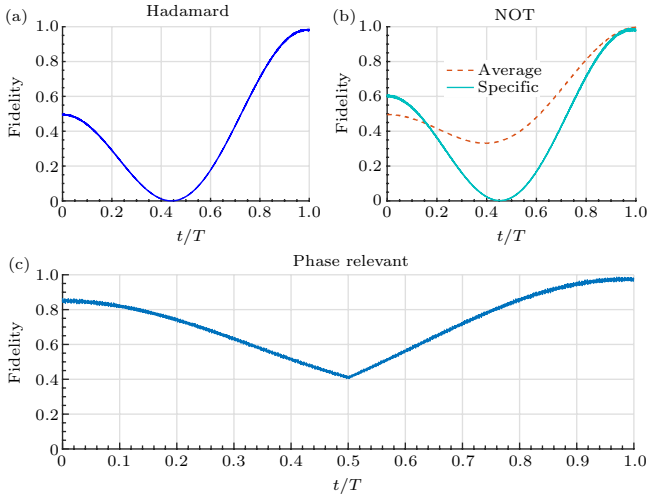


Fig. 3. Fidelity of the single-loop single-qubit NHQC during one evolution period: (a) Hadamard gate with $\vartheta = \pi/4$, $\theta = \pi/4$, $\gamma = \pi$, and $\varphi = \pi$; (b) NOT gate with $\vartheta = \pi/7$, $\theta = \pi/2$, $\gamma = \pi$, and $\varphi = \pi$ (solid line). The dashed line represents the average fidelity; (c) phase gate with $\vartheta = \pi/4$, $\theta = \pi/5$, $\gamma = \pi/4$, and $\varphi = \pi/3$. The parameters are chosen as $V \simeq 34.67\Omega_1$, $\Delta_1 = 10\Omega_1$, $\Delta_2 \simeq 23.33\Omega_1$, $\delta = -(4/3)\Omega_1$, $\Omega_2 = \Omega_1$, $\Omega_3 = \Omega_4 = \sqrt{\sin(\theta/2)}\Omega_1$, and $\Omega_5 = \Omega_6 = \sqrt{\cos(\theta/2)}\Omega_1$. Other parameters are chosen based on Eqs. (6) and (10).

In the discussion above, we ignored the RRI between atoms 2 and 3. In practice, the influence of V_{23} should also be discussed. In Fig. 4, we show the influence of V_{23} on the conventional single-qubit NHQC gate. The results show that the influence of V_{23} is negligible when $V_{23}/V \leqslant 0.4$. Experimentally, this influence can be effectively suppressed by engineering the spatial configuration of atoms, such that the distance between atoms 2 and 3 is larger than that between the nearest-neighbor pairs. Since the RRI scales strongly with distance, this leads to a significant reduction of V_{23}. In addition, the large-detuning conditions ensure that residual interactions only contribute as higher-order perturbative corrections to the effective Hamiltonian. Our numerical results in Fig. 4(b) further confirm that the gate fidelity remains high for $V_{23}/V \lesssim 0.4$, indicating that the scheme is robust against such imperfections. Therefore, the effect of V_{23} can be safely neglected under realistic experimental conditions.

We then consider the influence of decoherence through a non-Hermitian method described in Ref. [74], with the Hamil-

tonian becoming

$$\hat{H}_{\rm diss} = \hat{H} - {\rm i}\frac{\Gamma}{2}\sum_{j=1}^{6}\hat{\sigma}_j^{\dagger}\hat{\sigma}_j, \tag{19}$$

where $\hat{\sigma}_1 = |0\rangle_1\langle r|$, $\hat{\sigma}_2 = |1\rangle_1\langle r|$, $\hat{\sigma}_3 = |0\rangle_2\langle r|$, $\hat{\sigma}_4 = |1\rangle_2\langle r|$, $\hat{\sigma}_5 = |0\rangle_3\langle r|$, and $\hat{\sigma}_6 = |1\rangle_3\langle r|$. $\hat{H}$ includes the original Hamiltonian in Eq. (5) and the additional large-detuning interactions acting on the state $|1\rangle$. It is assumed that the Rydberg states of the three atoms have the same atomic spontaneous emission rate $\Gamma/2$ to the two ground states. In Fig. 5, we plot the single-qubit gate fidelity versus the dissipation rate, from which one can see that the fidelity remains higher than 0.9 even when the atomic spontaneous emission rate Γ/Ω_1 reaches 2×10^{-3}.

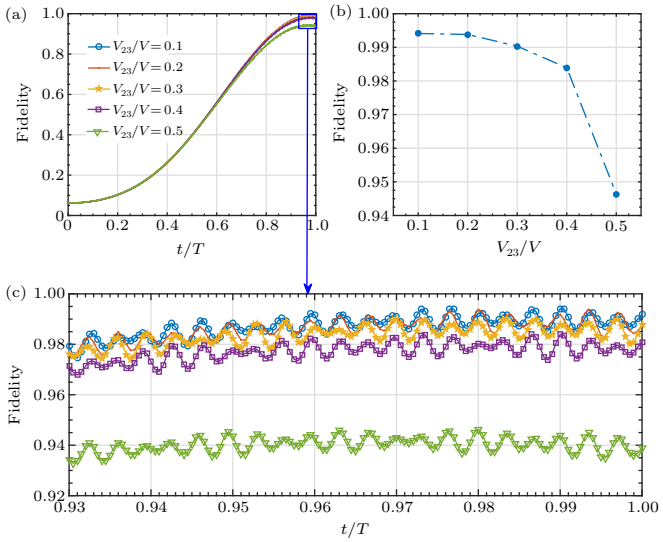


Fig. 4. (a) [(c)] The fidelity of the single-qubit NHQC gate $\hat{U}(\pi/4,\ \pi/3)$ for different V_{23} values as a function of evolution time. (b) The optimal fidelities as a function of V_{23}. The parameters are chosen as $\theta=\pi/4$, $\varphi=\pi/3$, and $\vartheta=\pi/8$. The remaining parameters are the same as those in Fig. 2.

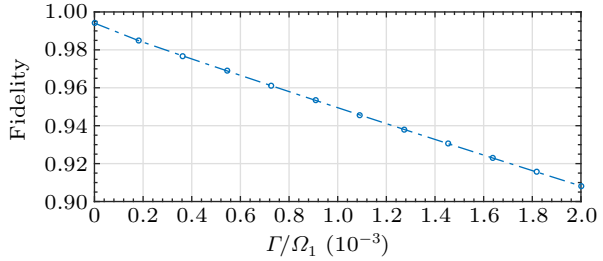


Fig. 5. Fidelity of the conventional single-qubit NHQC gate $\hat{U}(\pi/4,\ \pi/3)$ with $V_{23}/V=0.1$ as a function of the dissipation rate. The parameters are chosen as $\theta=\pi/4$, $\varphi=\pi/3$, and $\vartheta=\pi/8$. The remaining parameters are the same as those in Fig. 2.

4. Multi-logical-qubit holonomic gates

In the single-logical-qubit gates, the laser-coupled Rydberg states are adiabatically eliminated, so that unwanted Rydberg-state populations are strongly suppressed. However, in the multi-logical-qubit gates, the control logical qubits employ Rydberg-state encoding to provide the required conditional blockade. To construct two- and three-qubit holonomic gates in DFS, we take advantage of the asymmetric encoding. For the control logical qubit, we encode the DFS as $|0\rangle_L^c \equiv |0R\rangle_{c1c2}$, $|1\rangle_L^c \equiv |R0\rangle_{c1c2}$, while for the target logical qubit, we encode the same DFS as in the single-qubit case in Section 3, as shown in Fig. 6.

During the two-logical-qubit gate operation, no driving fields are applied to the control atoms, and the control logical qubit affects the target logical qubit through the Rydberg–Rydberg interaction. The full Hamiltonian can be written as

$$\hat{H}_{\rm 2q}(t) = \hat{H}_{\rm Ry}^{t}(t) + \hat{H}_{\rm add}^{t}(t) + \hat{H}_{\rm ct}, \tag{20}$$

where $\hat{H}_{\rm Ry}^{t}(t)$ is the target-qubit Rydberg-driving Hamiltonian

$$\hat{H}_{\rm Ry}^{t}(t) = \sum_{k=1}^{3}\left(\frac{\Omega_{2k-1}}{2}{\rm e}^{{\rm i}\Delta_{2k-1}t}|0\rangle_{t_k}\langle R| + \frac{\Omega_{2k}}{2}{\rm e}^{{\rm i}\Delta_{2k}t}|1\rangle_{t_k}\langle R| + {\rm H.c.}\right) + \sum_{1\le i<j\le 3} V_{t_it_j}|RR\rangle_{t_it_j}\langle RR|. \tag{21}$$

The term $\hat{H}_{\rm add}^{t}(t)$ denotes the additional large-detuned interactions used to compensate for the Stark shifts in the target logical qubit

$$\hat{H}_{\rm add}^{t}(t) = \sum_{l=2,3}\left(\frac{\Omega_{fl}}{2}{\rm e}^{{\rm i}\Delta_{fl}t}|1\rangle_{t_l}\langle f_l| + {\rm H.c.}\right). \tag{22}$$

The interaction between the control atoms and the target atoms is described by

$$\hat{H}_{\rm ct} = \sum_{\mu=1}^{2}\sum_{k=1}^{3} V_{c_\mu t_k}|R\rangle_{c_\mu}\langle R|\otimes|R\rangle_{t_k}\langle R|. \tag{23}$$

The above Hamiltonian leads to a controlled holonomic evolution of the target logical qubit. More specifically, the driving fields are applied only to the target logical qubit, while the control logical qubit remains unchanged during the gate operation. When the control logical qubit is in $|0\rangle_L^c$, atom c_2 is in the Rydberg state and produces a strong Rydberg blockade on the target atoms. As a result, the laser-induced transitions required for the target-qubit holonomic evolution are largely suppressed, and the target logical qubit undergoes an identity operation. In contrast, when the control logical qubit is in $|1\rangle_L^c$, the Rydberg excitation is located on atom c_1, whose interaction with the target atoms is designed to be negligible. In this case, the target logical qubit evolves under the effective Hamiltonian $\hat{H}_{\rm eff}^{t}$, i.e., Eq. (12), which is the same as that for the single-logical-qubit holonomic gate. Therefore, for an arbitrary two-logical-qubit input state $|\Psi(0)\rangle = |0\rangle_L^c\otimes|\phi_0\rangle_L^t + |1\rangle_L^c\otimes|\phi_1\rangle_L^t$, where $|\phi_0\rangle_L^t$ and $|\phi_1\rangle_L^t$ are arbitrary target-qubit states, the evolution after one cyclic period gives

$$|\Psi(T)\rangle = |0\rangle_L^c\otimes|\phi_0\rangle_L^t + |1\rangle_L^c\otimes\hat{U}^t(\theta,\varphi)|\phi_1\rangle_L^t.$$

Thus, the resulting two-logical-qubit operation is

$$\hat{\mathcal{U}} = |0\rangle_L^c\otimes\hat{I}_L^t + |1\rangle_L^c\otimes\hat{U}(\theta,\varphi)_L^t, \tag{24}$$

which realizes a controlled holonomic gate on the target logical qubit.

It is also noted that although Eq. (24) shows that universal two-logical-qubit operations can be constructed, how to realize single-logical-qubit operations in DFS^c should also be addressed. To do so, three steps are required. Step (i): Apply a π pulse to realize $|R\rangle \to |1\rangle$ of atom c_k $(k = 1,\ 2)$. Correspondingly, the state transformations $|0\rangle_L^c \to |01\rangle_c$ and $|1\rangle_L^c \to |10\rangle_c$ are realized. The states $|01\rangle_c$ and $|10\rangle_c$ remain in the collective-dephasing DFS. Step (ii): Apply the same lasers to atom c_k as those applied to atom k in Fig. 1. The effective Hamiltonian $\hat{H} = \lambda'|01\rangle_c\langle 10| + \text{H.c.}$ is achieved, based on which universal operations can be realized. Step (iii) is the inverse operation of Step (i).

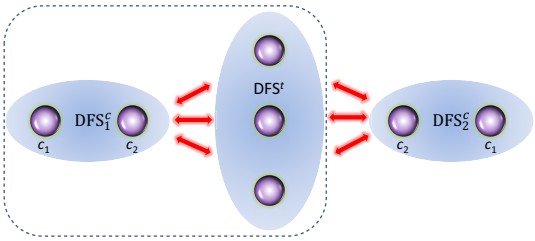


Fig. 6. Configuration for constructing two- and three-logical-qubit NHQC in DFS with asymmetric encoding: $|0\rangle_L \equiv |0R\rangle$ and $|1\rangle_L \equiv |R0\rangle$ for the control logical qubit subspace DFS$_j^c$ $(j = 1,\ 2)$, while $|0\rangle_L \equiv |001\rangle$ and $|1\rangle_L \equiv |100\rangle$ for the target logical qubit subspace DFS^t. The configuration enclosed by the dotted line denotes the two-logical-qubit case, while the entire configuration denotes the three-logical-qubit case.

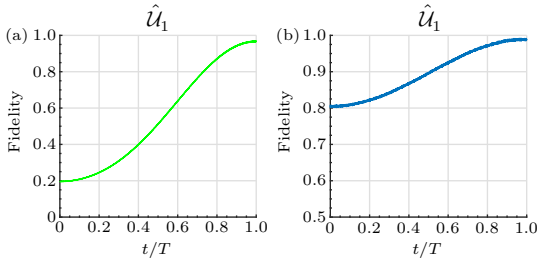


Fig. 7. The fidelity of the two-logical-qubit NHQC gate with the initial state $|\psi\rangle_L = \sin\alpha\sin\beta|0\rangle_L^c|1\rangle_L^t + \cos\alpha\sin\beta|0\rangle_L^c|0\rangle_L^t + \sin\alpha\cos\beta|1\rangle_L^c|1\rangle_L^t + \cos\alpha\cos\beta|1\rangle_L^c|0\rangle_L^t$. The parameters are chosen as $V \simeq 34.67\Omega_1, \Delta_1 = 13.3\Omega_1, \Delta_2 \simeq 20\Omega_1, \delta = -(4/3)\Omega_1, \Omega_2 = \Omega_1, \Omega_3 = \Omega_4 = \sqrt{\sin(\theta/2)}\,\Omega_1$, and $\Omega_5 = \Omega_6 = \sqrt{\cos(\theta/2)}\,\Omega_1$, with $\alpha = \pi/3$ and $\beta = \pi/3$. For $\hat{U}_1$, the remaining parameters are chosen as $\theta = \pi/4$ and $\varphi = \pi$. For $\hat{U}_2$, the parameters are chosen as $\alpha = \pi/3, \beta = \pi/3, \theta = \pi/2$, and $\varphi = \pi$.

To verify feasibility, we show the fidelities of two representative two-logical-qubit NHQC gates in Fig. 7. The fidelities exceed 0.98 and 0.99, respectively, at the end of the evolution, demonstrating that the conditional operation can be implemented with high fidelity. This verifies the feasibility of constructing two-logical-qubit holonomic gates by using the asymmetric encoding of the control logical qubit as a conditional blockade resource.

Generally, for a three-logical-qubit case, on the premise that conditions one and two are still satisfied for DFS$_2^c$, the evolution operator of the whole system can be expressed as

$$\hat{\mathbb{U}} = (|0\rangle_{L1}^c \otimes |0\rangle_{L2}^c + |0\rangle_{L1}^c \otimes |1\rangle_{L2}^c + |1\rangle_{L1}^c \otimes |0\rangle_{L2}^c) \otimes \hat{I}_L^t + |1\rangle_{L1}^c \otimes |1\rangle_{L2}^c \otimes \hat{U}(\theta,\varphi)_L^t. \tag{25}$$

$|0\rangle_{Lj}^c$ and $|1\rangle_{Lj}^c$ denote the logical qubit states in DFS$_j^c$. Equation (25) shows that the $\hat{\mathbb{U}}$ operation is applied to the target logical qubit if and only if both control logical qubits are in the state $|1\rangle_L$, indicating a universal three-logical-qubit operation. The scheme can be generalized to multi-qubit NHQC in DFS in a similar way.

5. Discussion and summary

In experiments, one can choose ^{87}Rb or ^{133}Cs atoms to realize the scheme. For Rb atoms, the ground states can be chosen as $|0\rangle \equiv |5S_{1/2},\ F = 1,\ m_F = 0\rangle$ and $|1\rangle \equiv |5S_{1/2},\ F = 2,\ m_F = 0\rangle$,[11] and the Rydberg state can be chosen as $|70S_{1/2}, m_J = -1/2\rangle$[16] for the two-photon excitation process. For Cs atoms, the ground states can be encoded in the hyperfine "clock states" $|0\rangle \equiv |6S_{1/2}, F = 4, m_F = 0\rangle$ and $|1\rangle \equiv |6S_{1/2}, F = 3, m_F = 0\rangle$,[75] and the Rydberg state can also be chosen with a principal quantum number n larger than 60.[15] In the above numerical simulations, we take $\Omega_1/2\pi = 3.5$ MHz as a realistic reference value.[16] Since the remaining parameters are given as dimensionless ratios with respect to Ω_1, their physical values can be obtained directly by rescaling according to these ratios.

In summary, we have proposed a scheme to implement nonadiabatic holonomic quantum computation within a decoherence-free subspace using Rydberg atoms. By encoding a logical qubit in the three-atom DFS spanned by $\{|001\rangle, |010\rangle, |100\rangle\}$, the scheme is inherently immune to collective dephasing noise. Working under the Rydberg antiblockade condition with large-detuned driving fields, all Rydberg states are adiabatically eliminated throughout the entire evolution, which not only minimizes errors due to atomic spontaneous emission but also largely suppresses the mechanical effects and sensitivity to interatomic distance variations associated with Rydberg excitations. Furthermore, by employing an asymmetric encoding strategy for the control and target qubits, we have extended the scheme to construct universal two- and three-logical-qubit holonomic gates, offering a scalable pathway toward multi-qubit geometric manipulation in Rydberg systems. Given its robustness against environment-induced decoherence, the present scheme may provide a promising route toward fault-tolerant quantum information processing with neutral atoms.

Acknowledgements

The author S. L. Su would like to thank Prof. K. Mølmer for valuable discussions. This work was supported by the Natural Science Foundation of Henan Province (Grant Nos. 262300422574, 262300421244, and 232300421075), the National Natural Science Foundation of China (Grant

Nos. 12304407, 62571494, 12575032, 12274376, and 12504497), the China Postdoctoral Science Foundation (Grant Nos. 2023TQ0310, GZC20232446, and 2024M762973), the Open Project of the State Key Laboratory of Metabolic Dysregulation & Prevention and Treatment of Esophageal Cancer (Grant No. 2025SGAQZ-QN-05), the Natural Science Foundation of Jiangsu Province (Grant Nos. BK20250404 and BG2025017), the Youth Science and Technology Talent Support Project of Jiangsu Province, and the Frontier Technology Research Program of Suzhou (Grant No. SYG202322).

References

[1] Gallagher T 1994 *Rydberg Atoms Cambridge Monographs on Atomic, Molecular and Chemical Physics* (Cambridge: Cambridge University Press)
[2] Jaksch D, Cirac J I, Zoller P, Rolston S L, Côté R and Lukin M D 2000 *Phys. Rev. Lett.* **85** 2208
[3] Lukin M D, Fleischhauer M, Cote R, Duan L M, Jaksch D, Cirac J I and Zoller P 2001 *Phys. Rev. Lett.* **87** 037901
[4] Saffman M, Walker T G and Mølmer K 2010 *Rev. Mod. Phys.* **82** 2313
[5] Saffman M 2016 *J. Phys. B* **49** 202001
[6] Comparat D and Pillet P 2010 *J. Opt. Soc. Am. B* **27** A208
[7] Wu X, Liang X, Tian Y, Yang F, Chen C, Liu Y C, Tey M K and You L 2021 *Chin. Phys. B* **30** 020305
[8] Urban E, Johnson T A, Henage T, Isenhower L, Yavuz D D, Walker T G and Saffman M 2009 *Nat. Phys.* **5** 110
[9] Gaëtan A, Miroshnychenko Y, Wilk T, Chotia A, Viteau M, Comparat D, Pillet P, Browaeys A and Grangier P 2009 *Nat. Phys.* **5** 115
[10] Wilk T, Gaëtan A, Evellin C, Wolters J, Miroshnychenko Y, Grangier P and Browaeys A 2010 *Phys. Rev. Lett.* **104** 010502
[11] Zhang X L, Isenhower L, Gill A T, Walker T G and Saffman M 2010 *Phys. Rev. A* **82** 030306
[12] Levine H, Keesling A, Omran A, Bernien H, Schwartz S, Zibrov A S, Endres M, Greiner M, Vuletić V and Lukin M D 2018 *Phys. Rev. Lett.* **121** 123603
[13] Ye G S, Xu B, Chang Y, Shi S, Shi T and Li L 2023 *Nat. Photonics* **17** 538
[14] Tan X, Wu J L, Deng C, Mao W J, Wang H T and Ji X 2018 *Chin. Phys. B* **27** 100307
[15] Madjarov I S, Covey J P, Shaw A L, Choi J, Kale A, Cooper A, Pichler H, Schkolnik V, Williams J R and Endres M 2020 *Nat. Phys.* **16** 857
[16] Levine H, Keesling A, Semeghini G, *et al.* 2019 *Phys. Rev. Lett.* **123** 170503
[17] Peper M, Li Y, Knapp D Y, Bileska M, Ma S, Liu G, Peng P, Zhang B, Horvath S P, Burgers A P and Thompson J D 2025 *Phys. Rev. X* **15** 011009
[18] Weimer H, Müller M, Lesanovsky I, Zoller P and Büchler H P 2010 *Nat. Phys.* **6** 382
[19] Jiao Y, Zhang Y, Bai J, Jia S, Adams C S, Bai Z, Shen H and Zhao J 2025 *Phys. Rev. Lett.* **135** 163603
[20] Chen T, Huang C, Velkovsky I, Ozawa T, Price H, Covey J P and Gadway B 2025 *Nat. Phys.* **21** 221
[21] Mølmer K, Isenhower L and Saffman M 2011 *J. Phys. B* **44** 184016
[22] Liu B B, Shan Z, Yun M R, Wang D Y, Liu B J, Yan L L, Feng M and Su S L 2022 *Phys. Rev. A* **106** 052610
[23] Wu J, Wu J L, Guo F Q, Liu B B, Su S L, Song X K, Ye L and Wang D 2025 *npj Quantum Inf.* **11** 118
[24] Ding D S, Liu Z K, Shi B S, Guo G C, Mølmer K and Adams C S 2022 *Nat. Phys.* **18** 1447
[25] Liang C, Yang C, Huang W and You L 2026 *Phys. Rev. Lett.* **136** 053203
[26] Wang Y J, Zhang J, Zhang Z Y, *et al.* 2026 *Nat. Commun.* **17** 1160
[27] Han Y, He B, Heshami K, Li C Z and Simon C 2010 *Phys. Rev. A* **81** 052311
[28] Liao R, Song Z R, Ye G S, Yu J H, Chang Y and Li L 2025 *Phys. Rev. Lett.* **135** 260803
[29] Zhang Y L, Jie Q X, Li M, Wu S H, Wang Z B, Zou X B, Zhang P F, Li G, Zhang T, Guo G C and Zou C L 2025 *Phys. Rev. Appl.* **24** 024052
[30] Berry M V 1984 *Proc. R. Soc. A* **392** 45
[31] Wilczek F and Zee A 1984 *Phys. Rev. Lett.* **52** 2111
[32] Aharonov Y and Anandan J 1987 *Phys. Rev. Lett.* **58** 1593
[33] Anandan J 1988 *Phys. Lett. A* **133** 171
[34] Jones J A, Vedral V, Ekert A and Castagnoli G 2000 *Nature* **403** 869
[35] Zanardi P and Rasetti M 1999 *Phys. Lett. A* **264** 94
[36] Duan L M, Cirac J I and Zoller P 2001 *Science* **292** 1695
[37] Wang X B and Keiji M 2001 *Phys. Rev. Lett.* **87** 097901
[38] Zhu S L and Wang Z D 2002 *Phys. Rev. Lett.* **89** 097902
[39] Sjöqvist E, Tong D M, Mauritz Andersson L, Hessmo B, Johansson M and Singh K 2012 *New J. Phys.* **14** 103035
[40] Xu G F, Zhang J, Tong D M, Sjöqvist E and Kwek L C 2012 *Phys. Rev. Lett.* **109** 170501
[41] Abdumalikov Jr A A, Fink J M, Juliusson K, Pechal M, Berger S, Wallraff A and Filipp S 2013 *Nature* **496** 482
[42] Egger D, Ganzhorn M, Salis G, Fuhrer A, Müller P, Barkoutsos P, Moll N, Tavernelli I and Filipp S 2019 *Phys. Rev. Appl.* **11** 014017
[43] Xu Y, Cai W, Ma Y, Mu X, Hu L, Chen T, Wang H, Song Y P, Xue Z Y, Yin Z q and Sun L 2018 *Phys. Rev. Lett.* **121** 110501
[44] Arroyo-Camejo S, Lazariev A, Hell S W and Balasubramanian G 2014 *Nat. Commun.* **5** 4870
[45] Zu C, Wang W B, He L, Zhang W G, Dai C Y, Wang F and Duan L M 2014 *Nature* **514** 72
[46] Sekiguchi Y, Niikura N, Kuroiwa R, Kano H and Kosaka H 2017 *Nat. Photonics* **11** 309
[47] Feng G, Xu G and Long G 2013 *Phys. Rev. Lett.* **110** 190501
[48] Ai M Z, Li S, He R, Xue Z Y, Cui J M, Huang Y F, Li C F and Guo G C 2022 *Fundamental Res.* **2** 661
[49] Kang Y H, Chen Y H, Shi Z C, Huang B H, Song J and Xia Y 2018 *Phys. Rev. A* **97** 042336
[50] Guo C Y, Yan L L, Zhang S, Su S L and Li W 2020 *Phys. Rev. A* **102** 042607
[51] Guo F Q, Wu J L, Zhu X Y, Jin Z, Zeng Y, Zhang S, Yan L L, Feng M and Su S L 2020 *Phys. Rev. A* **102** 062410
[52] Wu J L, Wang Y, Han J X, Jiang Y, Song J, Xia Y, Su S L and Li W 2021 *Phys. Rev. Appl.* **16** 064031
[53] Li M, Guo F Q, Jin Z, Yan L L, Liang E J and Su S L 2021 *Phys. Rev. A* **103** 062607
[54] Sun L N, Yan L L, Su S L and Jia Y 2021 *Phys. Rev. Appl.* **16** 064040
[55] Sun L N, Guo F Q, Shan Z, Feng M, Yan L L and Su S L 2022 *Phys. Rev. A* **105** 062602
[56] Wu J L, Wang Y, Han J X, Su S L, Xia Y, Jiang Y and Song J 2021 *Front. Phys.* **17** 22501
[57] Liang Y, Shen P, Chen T and Xue Z Y 2022 *Phys. Rev. Appl.* **17** 034015
[58] Xu J Z, Sun L N, Wei J F, Du Y L, Luo R, Yan L L, Feng M and Su S L 2022 *Chin. Phys. Lett.* **39** 090301
[59] Su S L, Sun L N, Liu B J, Yan L L, Yung M H, Li W and Feng M 2023 *Phys. Rev. Appl.* **19** 044007
[60] Su S L, Wang C, Song P Y and Chen G 2024 *Chin. Phys. Lett.* **41** 040302
[61] Sun H W, Wu J L and Su S L 2024 *Phys. Scr.* **99** 085122
[62] Song P Y, Wei J F, Xu P, Yan L L, Feng M, Su S L and Chen G 2024 *Phys. Rev. A* **109** 022613
[63] Liang Y, Tian X D, Ji L N and Xue Z Y 2025 *Phys. Rev. Appl.* **24** 034025
[64] Li J Q, Li H X, Song P Y, Wu J L, Liang Y and Su S L 2025 *Phys. Scr.* **100** 085123
[65] Guo F Q, Su S L, Li W and Shao X Q 2025 *Phys. Rev. A* **111** 022420
[66] Zanardi P and Rasetti M 1997 *Phys. Rev. Lett.* **79** 3306
[67] Brion E, Pedersen L H, Mølmer K, Chutia S and Saffman M 2007 *Phys. Rev. A* **75** 032328
[68] Zhang J, Kwek L C, Sjöqvist E, Tong D M and Zanardi P 2014 *Phys. Rev. A* **89** 042302
[69] Xue Z Y, Zhou J and Wang Z D 2015 *Phys. Rev. A* **92** 022320
[70] Liang Z T, Du Y X, Huang W, Xue Z Y and Yan H 2014 *Phys. Rev. A* **89** 062312
[71] Lee T E, Häffner H and Cross M C 2012 *Phys. Rev. Lett.* **108** 023602
[72] Su S L, Guo F Q, Wu J L, Jin Z, Shao X Q and Zhang S 2020 *Europhys. Lett.* **131** 53001
[73] Herterich E and Sjöqvist E 2016 *Phys. Rev. A* **94** 052310
[74] Shi X F 2019 *Phys. Rev. Appl.* **11** 044035
[75] Keating T, Goyal K, Jau Y Y, Biedermann G W, Landahl A J and Deutsch I H 2013 *Phys. Rev. A* **87** 052314